Combined HREM and HAADF Scanning Transmission Electron Microscopy: A Powerful Tool for Investigating Structural Changes in Thermally Aged Ceria−Zirconia Mixed Oxides

J. A. Pérez-Omil,[†] S. Bernal,[†] J. J. Calvino,*[,†] J. C. Hernández,[†] C. Mira,[†] M. P. Rodríguez-Luque,[†] R. Erni,[‡,§] and N. D. Browning[‡,§]

Departamento de Ciencia de los Materiales e Ingeniería Metalúrgica y Química Inorgánica, Facultad de Ciencias, Universidad de Cádiz, Campus Puerto Real, 11510 Cádiz, Spain, Department of Chemical Engineering and Materials Science, University of California−Davis, Davis, California 95616, NCEM, Lawrence Berkeley National Laboratory, Berkeley, California 94720

Received May 10, 2005
Revised Manuscript Received July 7, 2005

Ceria−zirconia mixed oxides are known to play a key role as redox components in the auto-exhaust three-way converters, one of the most successful developments of the catalysis technology over the last 30 years.[1]

The sensitivity of the redox response of ceria−zirconia mixed oxides to the thermal aging conditions is known to be a characteristic and very challenging feature of their behavior.[2−7] Heating these materials under flowing hydrogen at $T_{redn} \geq 1173$ K, followed by a mild ($T_{reoxn} \leq 873$ K) re-oxidation treatment, leads to highly reducible samples; whereas high-temperature ($T_{reoxn} \geq 1173$ K) re-oxidation results in a very significant deterioration of their reducibility.[3,6] Though considerable research effort has been devoted to the interpretation of this effect, some very recent publications clearly indicate that it is still a matter open to discussion.[4−6] In most of these studies the existence of a close relationship between the structural changes and redox properties is suggested to occur.[2,5−7] Rietveld analysis of X-ray powder diffractograms recorded for a $Ce_{0.50}Zr_{0.50}O_2$ sample reduced with pure H_2 at 1573 K, for 10 h, and further re-oxidized with pure O_2 at 873 K, supports the formation of a metastable κ-$CeZrO_4$ phase, resulting from the full re-oxidation of the pyrochlore, $Ce_2Zr_2O_7$, formed during the high-temperature reduction treatment.[2,7] Because cationic sublattice ordering is a characteristic feature of the pyrochlore phase, the proposal above suggests that, associated with high-temperature reduction treatment, a disorder−order transition in the cerium−zirconium sublattice occurs. Mild re-oxidation of the pyrochlore would keep this ordered cationic structure (κ phase), whereas high-temperature re-oxidation would destroy such an ordering effect.

To gain some further insight into this crucial question, a combination of high-resolution transmission electron microscopy (HREM) and atomic-resolution high-angle annular dark field scanning transmission electron microscopy (HAADF STEM) techniques have been applied. HREM images were recorded in a JEOL2000EX microscope operating at 200 kV. The structural resolution of this microscope is 0.21 nm. HAADF images were recorded in a Tecnai F20. Electron microscopy specimens were prepared by depositing the particles of the samples to be investigated onto holey carbon-coated 3-mm Cu grids. Deposition was achieved by dipping the grid directly into the powder of the samples, to avoid contact with any solvent, and further blowing off the excess powder.

Image analysis has been performed on digitized images using Digital Micrograph 3.4.3. Digital diffraction patterns (DDPs) shown here correspond to the log-scaled power spectrum of the corresponding fast Fourier transformations (FFTs). HREM images were digitized from negative plates using a COHU (768 × 512, 8 bits) charge coupled device camera. HAADF STEM images were directly digitized using the TIA (Tecnai Imaging & Analysis) interface implemented in the F20 microscope.

To build the supercell files of the structural models used as input in the HREM and HAADF image simulation tasks, the Rhodius code was used.[8] The calculation of the HREM image was done using the Multislice and image formation process routines of EMS.[9] The electronoptical parameters of a JEOL2000-EX microscope were used in these calculations ($C_s = 0.7$ mm, objective lens aperture diameter = 12 nm^{-1}, electron beam semi-convergence angle = 1.2 mrad, spread of focus = 10 nm, accelerating voltage = 200 kV). A nonlinear, partially coherent image formation process is assumed in the calculation. The calculation of the HAADF images was accomplished using the routines developed by Kirkland[10] with the following optical parameters: accelerating voltage = 200 kV; objective lens $C_s = 0.5$ mm; aperture diameter = 13.5 mrad; HAADF detector covering the 74−300 mrad range.

The oxide sample investigated here consisted of a texturally stabilized $Ce_{0.68}Zr_{0.32}O_2$, with 23 $m^2 \cdot g^{-1}$ specific surface

* To whom correspondence should be addressed. E-mail: jose.calvino@uca.es.
[†] Universidad de Cádiz.
[‡] University of California−Davis.
[§] Lawrence Berkeley National Laboratory.

(1) Shelef, M.; Graham, G. W.; McCabe, R. W. In *Catalysis by Ceria and related Materials*; Trovarelli, A., Ed.; Imperial College Press: London, 2002; Chapter 10, pp 343−375.
(2) Izu, N.; Omata, T.; Otsuka-Yao-Matsuo, S. *J. Alloys Compd.* **1998**, *270*, 107.
(3) Baker, R. T.; Bernal, S.; Blanco, G.; Cordón, A. M.; Pintado, J. M.; Rodríguez-Izquierdo, J. M.; Fally, F.; Perrichon, V. *Chem. Commun.* **1999**, 149.
(4) Fornasiero, P.; Moniti, T.; Graziani, M.; Kaspar, J.; Hungria, A. B.; Martínez-Arias, A.; Conesa, J. C. *Phys. Chem. Chem. Phys.* **2002**, *4*, 149.
(5) Montini, T.; Bañares, M. A.; Hickey, N.; Di Monte, R.; Fornasiero, P.; Kaspar, J.; Graziani, M. *Phys. Chem. Chem. Phys.* **2004**, *6*, 1.
(6) Montini, T.; Hickey, N.; Fornasiero, P.; Graziani, M.; Bañares, M. A.; Martínez-Huerta, M. V.; Alessandri, I.; Depero, L. E. *Chem. Mater.* **2005**, *17*, 1157.
(7) Kishimoto, H.; Omata, T.; Otsuka-Yao-Matsuo, S.; Ueda, K.; Hosono, H.; Kawazoe, H. *J. Alloys Compd.* **2000**, *312*, 94.
(8) Bernal, S.; Botana, F. J.; Calvino, J. J.; López Cartes, C.; Pérez-Omil, J. A.; Rodríguez-Izquierdo, J. M. *Ultramicroscopy* **1998**, *72*, 135.
(9) Stadelmann, P. *Ultramicroscopy* **1987**, *21*, 131.
(10) Kirkland, E. J. *Advanced Computing in Electron Microscopy*; Plenum Press: New York, 1998.

10.1021/cm050976g CCC: $30.25
Published on Web 07/23/2005

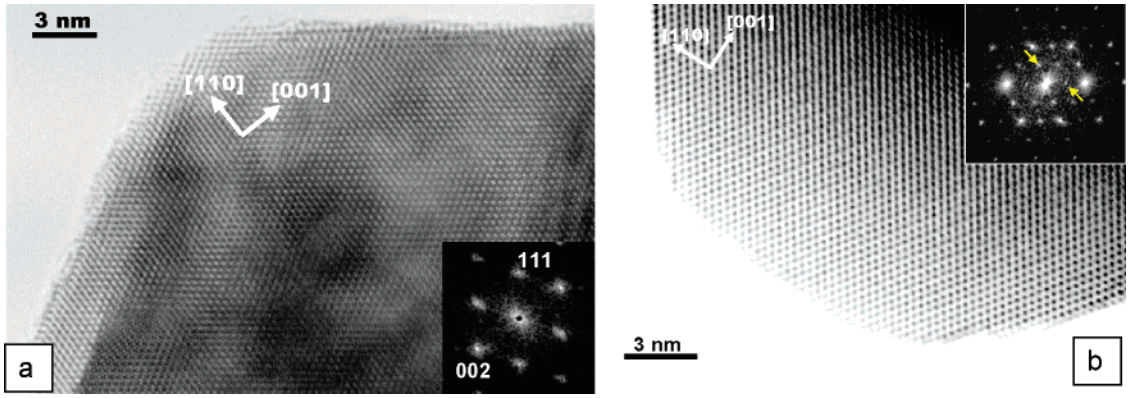

Figure 1. HREM images and DDPs corresponding to the fresh (a) and cycled (b) ceria−zirconia mixed oxide samples. Dots indicated by arrows in DDP of the cycled samples: 1/2 {111} superstructure reflections.

area. This oxide (fresh sample) was reduced under flowing 5% H_2/Ar at 1223 K, 1 h; then flushed for 1 h, at 1223 K, in a flow of He; and finally re-oxidized with flowing 5% O_2/He, at 823 K, 1 h (cycled sample). Additional characterization details about the fresh sample are reported elsewhere.[11]

Figure 1 shows representative HREM images of both fresh (a) and cycled (b) samples. The images were analyzed by means of FFT methods. DDPs obtained from these FFTs provide information about the spatial frequencies (lattice plane spacings) and their angular relationship in different zone axis orientations. As deduced from the DDP inset in Figure 1a, the fresh sample only shows the {111} and {002} reflections characteristic of the [110] orientation of a cubic, fluorite-type, mixed oxide. By contrast, the HREM image for cycled samples, Figure 1b, shows some additional features consisting of spots at 1/2 {111} positions. These extra reflections indicate the formation of a superstructure whose lattice parameters are twofold those of the original fluorite. HREM images showing the occurrence of superstructure features in ceria−zirconia mixed oxides have been reported earlier.[12−14] However, as deduced from Figure 2, the computer-simulated HREM image for a fluorite structure in which Ce^{4+} and Zr^{4+} are ordered in an alternate fashion along the three major ⟨001⟩ cubic cell directions shows the same superstructure features as those calculated for a structural model consisting of a random distribution of cations and an oxygen sublattice slightly distorted with respect to that of the ideal fluorite. We may conclude accordingly that the HREM technique cannot unambiguously interpret the superstructure contrasts observed in experimental HREM images such as the one shown in Figure 1b.

To clarify this critically important point, a parallel HAADF study has been performed. As is known, the HAADF image constrasts strongly depend on the average *Z* value in the atomic columns.[15,16] In the case of the ceria−zirconia

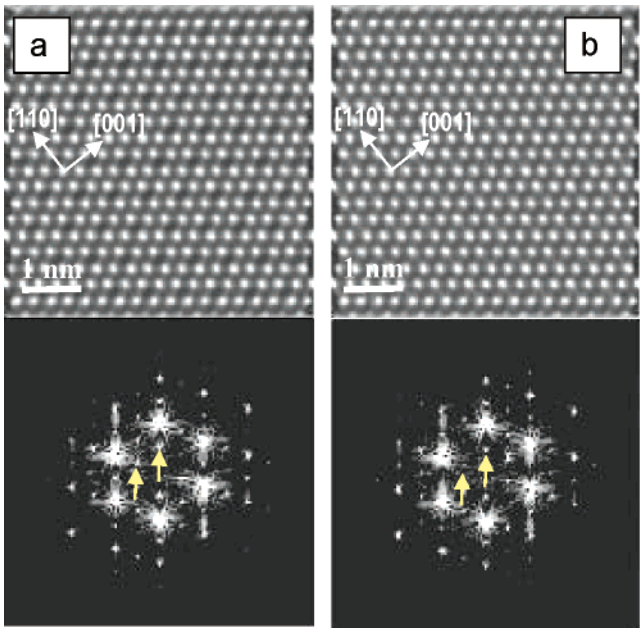

Figure 2. Computer-simulated HREM images for (a) a ceria−zirconia mixed oxide with fluorite structure and an ordered cationic sublattice and (b) a ceria−zirconia mixed oxide with Ce^{4+} and Zr^{4+} ions randomly distributed in the fluorite structure and the O^{2-} sublattice resulting from a slight distortion of the ideal fluorite structure. Notice that images a and b show the same superstructure features (extra 1/2 {111} spots in the DDPs).

samples, because of the high *Z* values for Ce ($Z = 58$) and Zr ($Z = 40$), bright contrasts would easily allocate the position of cationic columns. Moreover, the significant difference existing between the *Z* values for Ce and Zr would also allow us to detect the eventual changes occurring in the Ce and Zr distribution.

Figure 3a shows a representative atomic-resolution HAADF image of the cycled oxide. Superstructure features similar to those observed in Figure 1b are evident. In fact, the DDP recorded from this HAADF image, Figure 3b, contains also the 1/2 {111} superstructure spots. A closer look at the image reveals a contrast pattern consisting of very bright points at the corners of rhombi (see enlargement in Figure 3c), medium brightness points between them, along the edges of the rhombi, and finally, a darker one in the center of it. The intensity profiles shown in Figure 3d,e, recorded along the

(11) Colón, G.; Pijolat, M.; Valdivieso, F.; Vidal, H.; Kaspar, J.; Fonochio, E.; Daturi, M.; Binet, C.; Lavalley, J. C.; Baker, R. T.; Bernal, S. *J. Chem. Soc., Faraday Trans.* **1998**, *94*, 3717.
(12) Vidal, H.; Bernal, S.; Kaspar, J.; Pijolat, M.; Perrichon, V.; Blanco, G.; Pintado, J. M.; Baker, R. T.; Colon, G.; Fally, F. *Catal. Today* **1999**, *54*, 93.
(13) Torng, S.; Miyazawa, K.; Suzuki, K.; Sakuma, T. *Philos. Mag. A* **1994**, *70*, 505.
(14) Masui, T.; Ozaki, T.; Adachi, G.; Kang, Z.; Eyring, L. *Chem. Lett.* **2000**, *7*, 240.
(15) Pennycook, S. J.; Boatner, A. *Nature* **1988**, *336*, 565.
(16) Browning, N. D.; Arslan, I.; Moeck, P.; Topuria, T. *Phys. Status Solidi b* **2001**, *227*, 229.

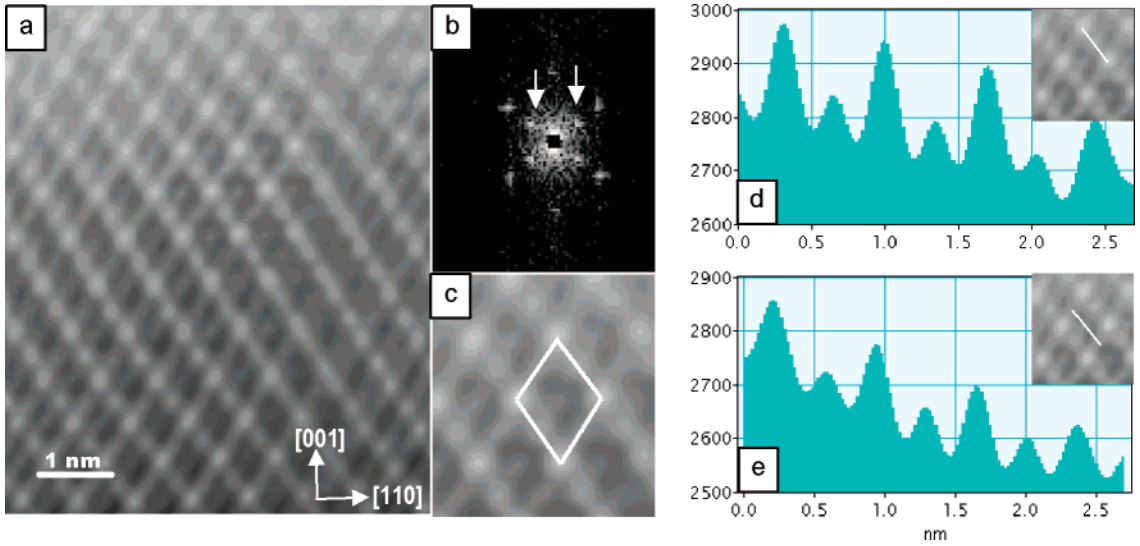

Figure 3. Experimental atomic-resolution HAADF image of the cycled oxide (a). DDP (b) confirms a [110] orientation of the oxide: the 1/2 {111} spots are indicated with arrows; (c) detail of the HAADF image (b). Intensity profiles along the rhombi edge (d) and along a parallel line passing through the rhombi center (e) are also included.

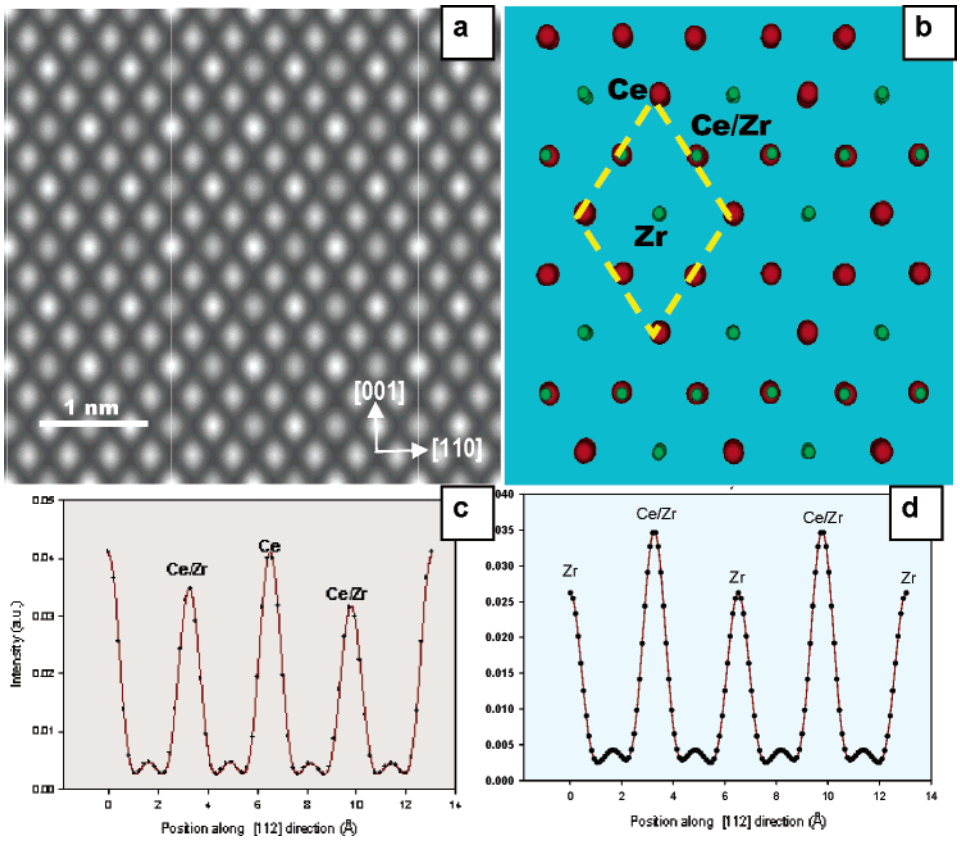

Figure 4. (a) Computer-simulated HAADF of a pyrochlore structure along the [110] zone axis (crystal thicknesss = 2 nm, $\Delta f = 434$ nm). (b) Projection in the [110] direction of the structural model used as input in the computer calculation of the HAADF image shown in part a. The rhombic net mentioned in the text is outlined. (c) Intensity profiles in the simulated image along the rhombi edge (c), Ce−(Ce + Zr)−Ce, and along a parallel line passing through the rhombi center (d), (Ce + Zr)−Zr−(Ce + Zr).

rhombi edge and along a parallel line passing through its center, clearly feature alternate intense and weaker peaks. The smooth and continuous change of the background in these profiles is very likely due to local thickness variations along the crystal. Likewise the slight distortions observed in the lower part of the image are simply an artifact due to the drift of the sample during the image acquisition time.

Taking into account the *Z* dependence of HAADF images, that, as revealed by both HREM and HAADF images, the basic fluorite structure is retained in the cycled oxide and that in the [110] zone axis orientation there is no overlap of cationic and anionic columns, we must conclude that the bright contrasts in the HAADF image correspond to purely cationic columns. Moreover, the intensity profiles show the existence of three different types of these cationic columns, thus, suggesting the occurrence of differences in their Ce/Zr contents. To confirm this proposal, a computer-simulated HAADF image has been generated by using as a model the

one of a pyrochlore phase, Figure 4a. Notice that, in the [110] projection of the fluorite superstructure of the pyrochlore, Figure 4b, three different types of purely cationic columns are found. Those located at the vertexes of the rhombic net (type 1) consist of Ce^{4+} cations exclusively, thus, leading to the brightest contrasts in Figure 4a. Type 2 columns mix Ce^{4+} and Zr^{4+} ions in an alternate fashion, thus, showing a lower average atomic number $[(Z_{Ce} + Z_{Zr})/2]$ and correspondingly lower brightness contrasts. They are located at half the edges of the rhombi. Finally, type 3 columns, those located in the center of the rhombic net, would only contain Zr^{4+} ions. As expected, they show the lowest spot intensity. All these observations are fully consistent with those resulting from the analysis of the experimental HAADF in Figure 3, thus, showing that, in the cycled sample, Ce^{4+} and Zr^{4+} cations have become ordered in an arrangement similar to the one occurring in the pyrochlore-related structure of the so-called κ phase.

To summarize, the combined application of HREM and HAADF techniques has allowed us to unambiguously interpretate the superstructure contrasts observed in the HREM images of a cycled ceria−zirconia mixed oxide. We may conclude, accordingly, that this approach offers a powerful tool for characterizing structural rearrangements occurring in the cationic sublattice of these materials. Moreover, compared to the macroscopic structural characterization techniques, like XRD or Raman spectroscopy, which are usually applied in the investigation of these phenomena,[2,5,6,7,17] the electron microscopy techniques offer some very specific advantages. In effect, they allow us to investigate these phenomena at a nanoscale, a critically important approach to fully understanding them.[18] Likewise, these electron microscopy techniques enhance our observation capabilities, thus, allowing us to detect these structural effects at earlier stages than those required by the macroscopic techniques mentioned above.[2,5,6,7,17]

Acknowledgment. MCYT (Project No. MAT2002-02782), the Junta de Andalucía (FQM334, FQM110), the Director Office of Science of the U.S. Department of Energy (Contract No. DE-AC03-76SF00098), and the Petroleum Research Fund (Contract No. 37552-AC5) are acknowledged for financial support

CM050976G

(17) Zhao, H.; Guillet, N.; Valdivieso, F.; Pijolat, M. *Solid State Ionics* **2003**, *160*, 317.
(18) Mamontov, E.; Brezny, R.; Koranne, M.; Egami, T. *J. Phys. Chem. B* **2003**, *107*, 13007.